ELSEVIER

Earth and Planetary Science Letters 173 (1999) 397–411

EPSL

www.elsevier.com/locate/epsl

Crystallization of the Zagami shergottite: an experimental study

Timothy J. McCoy [a,b,*], Gary E. Lofgren [b]

[a] *Department of Mineral Sciences, National Museum of Natural History, Smithsonian Institution, Washington, DC 20560-0119, USA*
[b] *Code SN4, NASA/Johnson Space Center, Houston, TX 77058, USA*

Received 15 June 1999; accepted 27 September 1999

Abstract

The Zagami meteorite is a Martian basalt which exhibits multiple lithologies formed by fractional crystallization. While the rock has been widely studied petrologically, its genesis is poorly constrained from an experimental standpoint. Ongoing debates about the thermal history of this and other Martian meteorites affect our thinking about the environments in which they could have formed (e.g. lava flow vs. subsurface dike) and the types of rocks that surficial Mars exploration are likely to recover. We report on twelve equilibrium and nine dynamic crystallization experiments on a synthetic Zagami composition. Equilibrium experiments run at temperatures of 1260–1050ºC yield results similar to those of previous workers [E.H. Stolper, H.Y. McSween Jr., Geochim. Cosmochim. Acta 43 (1979) 1475–1498]. We observe crystallization of ~40 wt.% of magnesian pyroxenes comparable in composition to the most magnesian pyroxene in Zagami, even though petrologic studies suggest that this magnesian pyroxene comprises only ~20 wt.% of the meteorite. Experiments run at a range of f_{O_2} from IW to QFM + 3.9 log units suggest that crystallization of Zagami under conditions as reducing as QFM − 3 log units cannot explain this discrepancy. Resorption of pyroxenes may have been an important factor in explaining this discrepancy. The most likely explanation is that Zagami crystallized from a melt with a higher Fe/Mg ratio than used in this work. Dynamic crystallization experiments run at a range of cooling rates (0.5–10ºC/h) and nuclei densities (1–3 vol.%, produced by varying the peak temperature between 1230º and 1250ºC) suggests that Zagami formed from a melt with a low nuclei density at a relatively slow cooling rate (<1ºC/h). Although these conditions produce a textural match for Zagami, important differences remain in the composition and chemical zoning of the experimental pyroxenes compared to Zagami. These differences might require either the use of a bulk composition with a higher Fe/Mg ratio or a slower (<0.1ºC/h) or multi-stage cooling rate. Published by Elsevier Science B.V.

Keywords: Zagami Meteorite; experimental studies; Mars; thermal history; crystallization; volcanism

1. Introduction

In the absence of returned Martian samples, the basaltic shergottite meteorites offer our best opportunity to understand volcanologic processes on Mars. Consequently, they have been the subject of numerous petrologic studies (e.g. [1–10]) and a few experimental studies (e.g. [1,11]) aimed at understanding their genesis. Perhaps the best studied of the basaltic shergottites is Zagami, a large (~18 kg) meteorite which fell in Nigeria in 1962 and became widely available through commercial sources around 1990. This rock contains multiple basaltic lithologies formed by fractional crystallization of a common parent magma [10].

* Corresponding author. Tel.: +1-202-357-2251; Fax: +1-202-357-2476; E-mail: mccoy.tim@nmnh.si.edu

0012-821X/99/$ – see front matter Published by Elsevier Science B.V.
PII: S0012-821X(99)00241-1

While this body of work has greatly enhanced our understanding of these meteorites, it has also pointed out a number of disagreements about the magmatic history of Zagami. Shergottitic pyroxenes contain magnesian cores that have been interpreted by some authors as cumulus (e.g. [1]). Experimental studies in which there have been attempts to crystallize pyroxene of this magnesian composition from a bulk shergottite melt have produced up to 40% crystals [1], while more recent petrologic studies [6,7,9] suggest the presence of only 10–20% of these crystals in shergottites. This difference has important implications for the degree of accumulation of pyroxene and the bulk composition of the melt from which these crystals formed.

Petrologic studies have also suggested two different crystallization histories. A two-stage magmatic history with Mg-rich pyroxene crystallization in a deep-seated (1–2 kbar) magma chamber followed by eruption of a thick, phenocryst-bearing lava flow was favored by [7], with cooling rates of ~0.1–0.02ºC/h [7,12]. A single-stage history with cooling at 5–20ºC/h was suggested by [6]. The debate about the thermal history experienced by Zagami is particularly critical, since the two different models require drastically different physical environments. Single-stage cooling at moderate rates can be accomplished in relatively thin lava flows. The multi-stage history probably requires volcanic edifices and thick lava flows or subsurface dikes [7]. Thus, understanding the history of individual shergottites significantly influences ideas about the types of surficial rocks likely to be encountered by future Mars missions.

The difference in Mg-rich pyroxene abundances, the possibility of a complex multi-stage history, and the lack of dynamic crystallization experiments to constrain the cooling rate of Zagami all suggested that a new experimental study was needed.

2. Experimental and analytical procedures

2.1. Starting material and run conditions

Starting material for the experiments was prepared from reagent-grade oxides and carbonates that were melted to a glass and ground to a fine powder. Charges were pressed from ~125 mg of starting glass, sintered onto ~5 mm diameter loops fabricated from 8 mil $Pt_{94}Rh_6$ wire, and run in a vertical Deltech furnace. Experiments were not run on iron pre-saturated Pt loops. Instead, the starting glass contains excess FeO (~1.5 wt.%) relative to the desired value. In all of the runs discussed here, the charge was held above the liquidus for 12–24 h to allow diffusion of iron from the charge into the Pt loop. This period of equilibration decreases the FeO concentration of the charge, producing the desired composition. After equilibration with a Pt loop at 1300ºC for 24 h, the starting composition closely matches the bulk composition of Zagami [7] (Table 1). Oxygen fugacity was controlled using a $CO–CO_2$ mixture. Reported oxygen fugacities are accurate to within ±0.2 log units. Temperatures were measured with Type B ($Pt_{94}Rh_6$–$Pt_{94}Rh_{30}$) thermocouples calibrated against the melting point of gold and are accurate to ±3ºC.

Table 1
Starting composition for experiments compared to bulk Zagami

	Starting composition	Zagami bulk composition [a]
SiO_2	51.3 (1)	51.2
TiO_2	0.81 (2)	0.81
Al_2O_3	6.18 (4)	6.19
FeO	17.8 (1)	18.2
MnO	0.55 (2)	0.55
MgO	10.3 (1)	10.4
CaO	10.6 (1)	10.7
Na_2O	1.29 (2)	1.29
K_2O	0.13 (1)	0.13
P_2O_5	0.56 (3)	0.58
Total	99.47	100.05

[a] Zagami composition from McCoy et al. [7].
Figures in parentheses are compositional variability of 10 analyses in last significant digit.

A variety of thermal histories were attempted for the equilibrium experiments to produce homogeneous grains of adequate size for analysis. We settled on a general thermal history which involved (a) melting at high temperature to equilibrate the charge and Pt loop, (b) cooling at a moderate rate to ~100ºC below the liquidus to produce crystals, (c) melting at 5–25ºC below the liquidus to destroy all but a few nuclei, and (d) equilibrating the charge at the final desired temperature. The specific thermal histories involved insertion of the charges into

the furnace at 1000ºC, raising the temperature at 1000ºC/h to 1270ºC, holding at 1270ºC for 12 h, cooling at 100ºC/h to 1150ºC and holding for 8 h, raising the temperature to 1230–1250ºC at 1000ºC/h and holding for 8 h, changing to the final temperature at 1000ºC/h and holding for 72 h. Samples were removed and quenched in compressed air. No evidence for growth of quench crystals in the experiments was observed.

Dynamic crystallization experiments were designed to vary both nuclei density and cooling rate. The thermal history involved (a) a high temperature phase (1270–1300ºC for 12+ h) to equilibrate the charge and Pt loop, (b) moderate cooling to 1150ºC and equilibration for 8 h to produce crystals, (c) melting at 5–25ºC below the liquidus (1250º, 1240º, 1230ºC) to destroy most nuclei, and (d) cooling at a range of rates (0.5–10ºC/h) to temperatures (900–1000ºC) below the solidus. We used constant cooling rates in our experiments for two reasons. Firstly, these experiments are the first dynamic crystallization experiments which have attempted to reproduce basaltic shergottite textures. For this reason, the simplest case, that of constant cooling, seemed an appropriate starting point. Secondly, for the outer portions of lava flows, the cooling rates are approximately linear between the liquidus and the solidus [13], excluding minor deviations caused by the heat of crystallization. This same effect occurs in the experiments, although it is mitigated by the control on temperature of the furnace. For each remelting temperature, a charge was run and removed after step (c) to examine the size, shapes, and distribution of the nuclei prior to cooling.

2.2. Analytical techniques

Phases (glass, augite, pigeonite, olivine) were analyzed using the JEOL JXA-8900R electron microprobe in the Department of Mineral Sciences at the Smithsonian Institution. Well-known standards and standard analytical conditions were used. Pyroxenes were analyzed with a fully focused beam (~1 μm), while glass was analyzed with a 10 μm diameter beam. Proportions of phases in equilibrium charges (Table 3) were determined from the bulk composition and average compositions of the individual phases using a least-squares mixing model.

3. Equilibrium experiments

We report results on twelve experiments designed to produce equilibrium assemblages at a range of temperatures and oxygen fugacities.

3.1. Effect of temperature

Equilibrium experiments were run at a range of temperatures from 1260º to 1050ºC. The liquidus for this composition was found to be between 1255º and 1260ºC with pigeonite as the liquidus phase. Compositions of glass, pigeonite and augite are given in Table 2. Table 3 is a summary of run conditions, abundances of phases, and end-member compositions for the various phases. At 1255ºC, pigeonite is homogeneous and relatively magnesian, with a composition of $Fs_{21.0}Wo_{5.0}$. Least-squares mixing calculations suggest that pigeonite comprises ~1% of the charge at 1255ºC. Minor olivine ($Fa_{24.2}$) is also present. These phases coexist at 1255º, 1240º and 1230ºC and become systematically more iron-rich and more abundant. Augite appears at 1175ºC. At this temperature, pigeonite has become appreciably more abundant (15 wt.%), as well as iron- and calcium-rich ($Fs_{26.0}Wo_{12.0}$). It is also somewhat less homogeneous between and within grains. Both pigeonite and augite are present from 1175ºC to 1050ºC, becoming more abundant and iron-rich and less homogeneous (Tables 2 and 3). Traces of FeO-rich olivine ($Fa_{49–54}$) are present at 1100º and 1050ºC. At the lowest temperatures, we did not observe the crystallization of feldspar or other interstitial phases.

The attainment of equilibrium is a significant concern in these experiments. At temperatures of 1200ºC and above, preliminary experiments were equilibrated for 24 h. Comparison of the 24 h and 72 h runs allows us to evaluate the approach to equilibrium. The compositions of these 24 h runs do not differ from those of the 72 h runs reported here. This might suggest that either equilibrium was obtained in time spans as short as 24 h or that cation diffusion is slow enough that equilibrium was not obtained in 72 h. We favor the former interpretation because of the excellent agreement between our crystallization experiments and the partial melting experiments of [1], as discussed below. At lower temperatures, equilibrium becomes a more serious concern. At 1150ºC,

Table 2
Average compositions of glass, pigeonite and augite from equilibrium crystallization experiments

Exp.	T (°C)	f_{O_2}	Na_2O	Al_2O_3	FeO	K_2O	TiO_2	MgO	SiO_2	MnO	CaO	P_2O_5	Total
Glass													
053	1260	QFM	1.04 (5)	6.16 (3)	17.1 (2)	0.07 (2)	0.83 (2)	10.6 (1)	51.7 (2)	0.56 (5)	10.4 (1)	0.51 (4)	98.99
054	1255	QFM	1.06 (6)	6.12 (13)	17.2 (3)	0.06 (1)	0.83 (1)	10.5 (1)	51.0 (6)	0.54 (5)	10.4 (1)	0.51 (5)	98.26
051	1240	QFM	1.16 (5)	6.34 (12)	17.1 (4)	0.07 (2)	0.86 (2)	9.98 (13)	51.2 (5)	0.55 (4)	10.7 (1)	0.54 (4)	98.51
049	1230	QFM	1.23 (7)	6.52 (10)	17.3 (2)	0.08 (2)	0.86 (2)	9.63 (13)	51.6 (2)	0.56 (3)	10.9 (1)	0.58 (4)	99.29
055	1200	QFM	1.38 (4)	7.24 (5)	17.7 (3)	0.10 (2)	0.95 (1)	7.88 (13)	50.9 (2)	0.54 (6)	11.4 (1)	0.66 (4)	98.76
056	1175	QFM	1.78 (5)	7.95 (8)	18.8 (3)	0.12 (2)	1.04 (2)	6.78 (9)	50.1 (2)	0.56 (3)	10.8 (1)	0.78 (5)	98.69
074	1150	QFM	2.06 (5)	9.20 (14)	19.2 (5)	0.20 (2)	1.15 (3)	5.28 (19)	49.0 (3)	0.52 (3)	10.2 (1)	0.89 (5)	97.72
075	1100	QFM	2.89 (6)	11.9 (1)	17.1 (5)	0.29 (3)	1.33 (2)	3.62 (13)	50.3 (4)	0.41 (4)	8.71 (8)	1.18 (4)	97.68
076	1050	QFM	3.16 (18)	13.8 (5)	14.6 (5)	0.38 (3)	1.33 (5)	2.92 (61)	52.8 (2)	0.37 (1)	7.65 (17)	1.49 (7)	98.57
077	1150	IW	1.73 (5)	9.57 (7)	18.1 (2)	0.18 (2)	1.18 (2)	5.28 (6)	50.4 (2)	0.55 (3)	10.5 (1)	0.79 (4)	98.24
063	1150	QFM + 2	2.01 (9)	8.66 (10)	19.8 (2)	0.19 (2)	1.12 (2)	5.60 (15)	48.8 (2)	0.52 (4)	9.95 (9)	0.85 (5)	97.47
064	1150	QFM + 3.9	2.31 (16)	9.58 (5)	9.48 (22)	0.26 (3)	1.07 (2)	4.95 (8)	59.9 (2)	0.43 (2)	8.23 (9)	1.08 (4)	97.29
Pigeonite													
054	1255	QFM	b.d.	0.25 (3)	13.6 (2)	b.d.	0.10 (1)	26.8 (3)	55.4 (3)	0.56 (5)	2.54 (8)	b.d.	99.75
051	1240	QFM	b.d.	0.26 (3)	13.9 (3)	b.d.	0.10 (2)	26.4 (2)	55.4 (2)	0.60 (4)	2.89 (15)	b.d.	99.53
049	1230	QFM	b.d.	0.28 (2)	14.3 (3)	b.d.	0.11 (1)	26.1 (1)	55.6 (1)	0.61 (2)	3.09 (8)	b.d.	100.12
055	1200	QFM	b.d.	0.41 (9)	15.0 (4)	b.d.	0.14 (2)	23.3 (1.1)	54.6 (3)	0.65 (4)	5.5 (1.3)	b.d.	99.60
056	1175	QFM	b.d.	0.61 (19)	16.4 (6)	b.d.	0.15 (2)	21.9 (8)	53.7 (3)	0.67 (4)	5.89 (61)	b.d.	99.33
074	1150	QFM	b.d.	1.03 (55)	18.9 (4)	b.d.	0.22 (8)	19.7 (4)	53.1 (2)	0.72 (3)	6.80 (84)	b.d.	100.51
075	1100	QFM	0.07 (3)	1.41 (52)	23.0 (6)	b.d.	0.28 (4)	17.6 (5)	52.2 (4)	0.80 (5)	5.53 (84)	b.d.	100.86
076	1050	QFM	0.10 (4)	1.62 (41)	23.9 (1.2)	b.d.	0.39 (8)	16.2 (5)	51.7 (2)	0.77 (5)	6.4 (1.6)	b.d.	101.14
077	1150	IW	b.d.	0.83 (28)	17.4 (2.2)	b.d.	0.22 (5)	21.8 (2.4)	54.4 (6)	0.69 (8)	5.6 (1.2)	b.d.	100.86
063	1150	QFM + 2	0.06 (3)	0.63 (24)	16.1 (2.4)	b.d.	0.13 (4)	23.8 (3.0)	54.5 (1.1)	0.69 (8)	4.6 (1.4)	b.d.	100.48
Augite													
056	1175	QFM	0.12 (1)	1.01 (11)	12.3 (8)	b.d.	0.21 (2)	17.4 (7)	53.0 (3)	0.53 (5)	14.7 (1.5)	b.d.	99.27
074	1150	QFM	0.13 (3)	1.12 (10)	14.6 (3)	b.d.	0.23 (2)	16.4 (1)	52.8 (2)	0.58 (3)	14.1 (4)	b.d.	100.03
075	1100	QFM	0.22 (6)	2.59 (66)	16.8 (9)	b.d.	0.54 (13)	12.7 (1.3)	60.0 (6)	0.64 (5)	16.2 (1.7)	b.d.	100.79
076	1050	QFM	0.21 (2)	3.05 (26)	17.4 (8)	b.d.	0.67 (8)	12.3 (9)	50.6 (4)	0.61 (5)	16.0 (1.3)	0.10 (6)	100.94
077	1150	IW	0.09 (2)	1.69 (27)	14.9 (6)	b.d.	0.38 (6)	17.0 (1.0)	53.2 (3)	0.63 (5)	12.9 (1.3)	b.d.	100.83
063	1150	QFM + 2	0.20 (2)	1.68 (27)	13.2 (6)	b.d.	0.26 (3)	16.4 (7)	52.6 (3)	0.56 (4)	15.4 (1.2)	b.d.	100.32
064	1150	QFM + 3.9	0.28 (2)	2.44 (47)	10.0 (2.4)	b.d.	0.33 (7)	17.7 (9)	51.8 (1.0)	0.65 (4)	16.9 (1.8)	b.d.	100.11

Numbers in parentheses are analytical variability in the last significant figure(s).

Table 3
Summary of equilibrium experiments

Exp.	T (ºC)	f_{O_2}	Glass	Pigeonite			Augite			Olivine	
			wt.%	wt.%	Fs	Wo	wt.%	Fs	Wo	wt.%	Fa
053	1260	QFM	100								
054	1255	QFM	99	1	21.0 (3)	5.0 (2)				Tr	24.2
051	1240	QFM	98	1	21.5 (4)	5.7 (3)				1	24.9
049	1230	QFM	96	3	22.1 (3)	6.1 (1)				1	26.0
055	1200	QFM	85	15	23.6 (6)	11.2 (2.7)					
056	1175	QFM	73	15	26.0 (9)	12.0 (1.3)	12	19.9 (1.3)	30.2 (3.2)		
074	1150	QFM	59	19	30.1 (6)	13.9 (1.7)	22	23.6 (5)	29.2 (7)		
075	1100	QFM	40	22	37.4 (8)	11.5 (1.8)	38	28.0 (1.4)	34.5 (3.7)	Tr	48.5
076	1050	QFM	33	25	39.2 (1.9)	13.5 (3.4)	42	29.0 (1.3)	34.3 (3.0)	Tr	53.8
077	1150	IW	62	13	27.4 (3.8)	11.4 (2.5)	25	24.1 (1.0)	26.8 (2.9)		
074	1150	QFM	59	19	30.1 (6)	13.9 (1.7)	22	23.6 (5)	29.2 (7)		
063	1150	QFM + 2	63	13	25.1 (4.3)	9.3 (2.6)	24	21.2 (9)	31.7 (2.6)		
064	1150	QFM + 3.9	X					15.8 (3.8)	34.3 (3.7)		

Tr = trace of mineral present; X = present, modes not determined for exp. 064.

compositional variability is less than or equal to 2% of the average of FeO and MgO in both augite and pigeonite. By 1050ºC, compositional variability is still less than or equal to 6% of the average of FeO and MgO. Given these rather small compositional variabilities and the larger differences in compositions between temperatures, we argue that equilibrium was achieved above 1200ºC and closely approximated below 1200ºC.

An important goal of this work was to determine the abundance of pigeonite and augite present in the experimental charges when the compositions of these phases match the natural magnesian 'cores' observed in Zagami. In natural Zagami, these cores occupy ~10 vol.% each of pigeonite and augite with compositions of $Fs_{29–31}Wo_{12}$ and $Fs_{20}Wo_{32}$, respectively [1,7]. The best compositional match to natural Zagami is observed in our 1150ºC charge. In this charge, pigeonite ($Fs_{30.1}Wo_{13.9}$) occupies 19 wt.% of the charge and augite ($Fs_{23.6}Wo_{29.2}$) comprises 22 wt.%.

3.2. Comparison with Stolper and McSween [1]

While several studies have measured or inferred the abundance of magnesian cores in Shergotty and Zagami [6,7,9], only a single experimental equilibrium study of shergottites has been previously conducted [1]. Comparison of our results with theirs shows that the two sets of experiments are remarkably similar (Table 4), despite differences in experimental method. We performed equilibrium crystallization experiments on a synthetic Zagami composition, while [1] conducted partial melting experiments on natural Zagami and Shergotty. The two sets of experiments produced similar liquidus temperatures (1255–1260º vs. 1240ºC), both observed pigeonite as the liquidus phase with similar compositions at the liquidus (Fs_{21} vs. Fs_{22}), both observed the onset of augite crystallization at nearly identical temperatures (1175º vs. 1176ºC), and they produced similar abundances of magnesian pyroxenes at compositions similar to those in natural Zagami cores (41 vs. 45 wt.%). Fig. 1 plots our phase abundance data for glass, pigeonite and augite. Solid lines are trends in phase abundance from [1]. In large part, our modal data are essentially identical to [1]. Some differences do exist and these might be important. We did not observe either plagioclase crystallization or complete solidification at the solidus. This lack of low-temperature crystallization almost certainly results from difficulties in nucleating these phases [14,15]. In natural magmas, melt movement may play a considerable role in influencing crystallization behavior [16]. Plagioclase is present at low temperatures in the experiments of [1], but these were partial melting experiments in which the plagioclase was already present in the starting material and the temperature was insufficient to completely melt this phase. As

Table 4
Comparison of our equilibrium experiments with natural Zagami and the experiments of Stolper and McSween [1]

	Natural Zagami	This work	S & M
Liquidus (ºC)		1255–1260	1240
Liquidus phase		Pigeonite	Pigeonite
Liquidus pigeonite composition		$Fs_{21.0}Wo_{5.0}$	$Fs_{22}Wo_{7}$
Augite onset (ºC)		1175	1176
Pyroxene comps. match (ºC)		1150	1140
Mg-rich cores in Zagami			
Pigeonite (wt.%)	~10%	19	22
Pigeonite comp.	$Fs_{29–31}Wo_{12}$	$Fs_{30.1}Wo_{13.9}$	~$Fs_{29}Wo_{12}$
Augite (wt.%)	~10%	22	23
Augite comp.	$Fs_{20}Wo_{32}$	$Fs_{23.6}Wo_{29.2}$	$Fs_{22}Wo_{32}$
Glass (wt.%)		59	55
Plagioclase crystallization (ºC)		Not observed	1082–1105
Solidus (ºC)		Not observed	1062?

a result, we see a higher proportion of glass in our charges at low temperatures than [1]. A more interesting difference is that [1] reported the presence of opaque phases (presumably Fe,Ti-oxides) even at the liquidus. In contrast, we did not observe Fe,Ti-oxides in any of our experiments run at QFM.

3.3. Explanations for the experimental vs. petrologic conundrum

We are left with the problem that equilibrium crystallization experiments produce ~40 wt.% magnesian pyroxene, while Zagami itself contains only

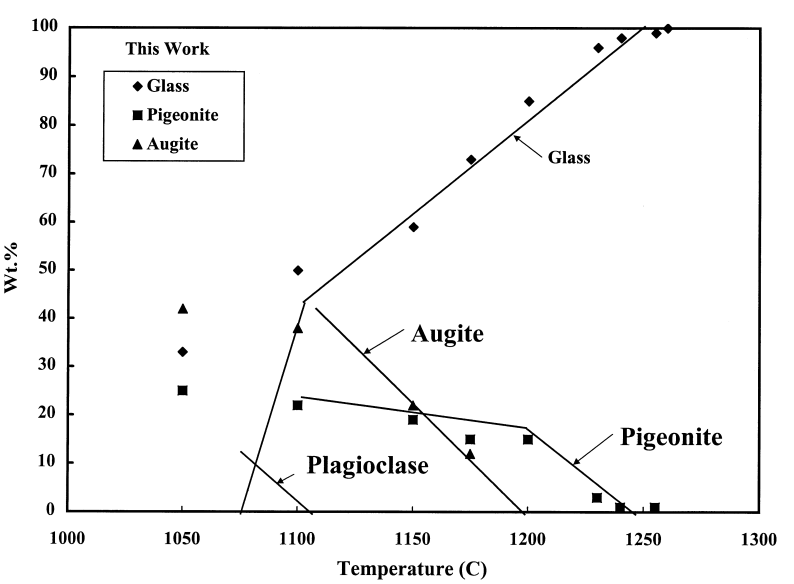

Fig. 1. Proportions of phases present in the equilibrium crystallization experiments from our work (symbols) and [1] (solid lines taken from their work). In general, the agreement in phase proportions is excellent. Below 1100ºC, we did not nucleate feldspar and, thus, see a higher proportion of glass than [1].

~20 wt.%. Several possible explanations have been offered to explain the difference between petrologic and experimental studies.

3.3.1. Homogenization and rapid crystallization

Three possibilities to explain why the first crystallizing pyroxenes in the experiments were significantly more magnesian than in natural Zagami were suggested by [1], although they did not address the issue of magnesian pyroxene abundances. Among these were (1) that FeO-rich pyroxenes crystallized during rapid crystallization rather than at equilibrium conditions, and (2) that early magnesian cores were homogenized during slow cooling. Rapid cooling seems an unlikely explanation. Detailed petrologic [6,7] and experimental studies (see below) suggest that rapid cooling did not occur, making the last possibility unlikely. While early-formed pyroxenes almost certainly homogenized during slow cooling, pyroxene would continue to crystallize during this period of slow cooling and, thus, the discrepancy in abundances cannot be explained by this mechanism. Homogenization of early-formed pyroxenes with the evolving melt might explain why pigeonite and augite appear to be in equilibrium with a common melt composition [1], yet do not appear on the liquidus together.

3.3.2. Oxygen fugacity

The experiments of [1] (run at QFM) may have been conducted at oxygen fugacities more oxidizing than were present during the crystallization of the basaltic shergottites. Indeed, shergottites might have crystallized at more reducing conditions (QFM − 3) than typically accepted (QFM) for these rocks [17], although this suggestion has been refuted by [9]. Could conditions as reducing as QFM − 3 explain the discrepancy between petrologic and experimental results? To evaluate these possibilities, we conducted experiments with our Zagami bulk composition at 1150ºC (the temperature at which we best matched the natural magnesian pyroxenes at QFM) at oxygen fugacities of IW (iron–wüstite), QFM, QFM + 2, and QFM + 3.9 (pure CO_2 in our CO–CO_2 mixing apparatus). Results of these experiments are given in Tables 2 and 3. Experiments conducted at conditions between IW and QFM + 2 showed no significant differences in pyroxene compositions or abundances, with ranges in total pyroxene abundances from 37 to 41 wt.%. Note that an oxygen fugacity of QFM − 3 is 0.5 log units above IW at 1150ºC. The only significant difference is seen at QFM + 3.9, when Fe-oxides precipitated from the silicate melt and the subsequent silicate melt crystallized only pigeonite of much more magnesian composition. As long as the oxygen fugacity is within the range at which FeO is neither oxidized nor reduced out of the silicate melt, differences in oxygen fugacity cannot explain the petrologic vs. experimental conundrum. A similar conclusion was recently reached by [18].

Could overly oxidizing conditions have altered the results of [1]? The presence of Fe,Ti-oxides in their experiments and the absence of these phases in our experiments at QFM suggest that their experiments might have experienced conditions more oxidizing than QFM. While [1] may have performed their experiments at conditions which were too oxidized, it did not have a significant effect, a conclusion supported by the similarity between our two experimental sets.

3.3.3. Pressure effects

Is it possible that crystallization at pressure might explain the discrepancy? Crystallization of the magnesian pyroxenes at moderate pressures (1–2 kbar) has been suggested [7], although this conclusion has been called into question by subsequent workers [19,20]. The role of pressure has been evaluated by [9] using the MELTS program to calculate the crystallization of a Shergotty bulk magma at moderate pressures. These authors found that the proportion of pyroxene crystallized is actually higher at 2 kbar than at 1 bar, not lower as might be predicted. However, these results should be viewed with caution, for [9] note that the MELTS program fails to predict pyroxene multiple saturation in either case, contrary to observations in Shergotty.

3.3.4. Resorption of pyroxenes

Many of the magnesian cores of pyroxenes in Zagami exhibit re-entrant textures at their edges, suggesting to [12] that resorption of these magnesian pyroxenes, with subsequent overgrowth by more FeO-rich pyroxene, had occurred. A plausible physical scenario in which this could have occurred was proposed by [7]. In their model, the magnesian cores

grew at depth and were subsequently entrained in a rising magma. Eruption of this phenocryst-bearing magma to a near-surface environment [7] could have caused a pressure-induced (not compositionally induced) shift in phase boundaries, resulting in resorption of early-formed, magnesian pyroxene. Could ~20% of the magnesian cores have been resorbed to explain why experimental results suggest ~40% magnesian pyroxene, but petrologic studies find only ~20% of this pyroxene? We can examine this idea by considering thermal constraints on assimilation following the approach of [8] to examine assimilation of lherzolite xenoliths in EET A79001. Zagami consists of ~80% pyroxene (both pigeonite and augite) and ~20% plagioclase [7]. A simplified model for assimilation would consist of 40 g of pyroxene and 60 g of melt. Melting 20% of the pyroxene would require 12.3 kJ, using a heat of fusion for orthopyroxene of 616 J/g [21]. Crystallization of the remaining 60 g of melt (40 g pyroxene, 20 g feldspar) would produce 23.6 kJ, using latent heats of crystallization for clinopyroxenes of ~430 J/g and for plagioclase of ~322 J/g [21]. This is almost certainly an upper limit, as assimilation is not operable at high degrees of crystallization [8]. Thus, it is clear that resorption could have played a significant role in explaining the petrologic vs. experimental discrepancy. Direct physical evidence for resorption is discussed later in Section 4. We doubt, however, that this is the only factor in explaining the discrepancy.

3.3.5. Bulk composition

If we had used a melt composition with a higher Fe/Mg ratio than Zagami's bulk composition, one of the natural consequences would have been a reduction in the percentage of magnesian cores. The liquidus pigeonite of this melt would have been FeO-enriched compared to the liquidus pigeonite in our experiments ($Fs_{21.0}$) and a smaller volume of pyroxene would crystallize at compositions comparable to those in Zagami. There is considerable evidence that Zagami did crystallize from a melt with a higher Fe/Mg ratio than used in this work. Several authors, most notably [1], have argued that magnesian pyroxenes in Shergotty and Zagami are cumulus grains that were in equilibrium with an intercumulus melt and that this intercumulus melt is a better approximation of the bulk composition. In the experiments of [1], this intercumulus melt (the glass in experiment Za-76) is enriched by 1.2 wt.% in FeO relative to the bulk and, more importantly, has an FeO/MgO ratio of 3.8 compared to a ratio of 1.6 in bulk Zagami. In our experiments, the intercumulus melt has an FeO/MgO ratio of 3.6 at 1150ºC. Further evidence of an FeO-enriched melt comes from recent petrologic studies. FeO-enriched lithologies occur in the main mass of Zagami [10]. Calculation of a bulk composition for Zagami which includes these lithologies in abundances found in the main mass suggest a bulk melt enriched by ~1 wt.% FeO [10].

It seems an inescapable conclusion that the bulk of Zagami is a cumulate rock and that its bulk composition does not reflect the composition of the melt from which the rock crystallized. Bulk composition may well be the main reason for the experimental vs. petrologic discrepancy. It seems possible that if the 'correct' bulk composition could be ascertained, it might be possible to crystallize Zagami from this composition. While fractional crystallization and crystal settling must have played a role, and magma migration might have resulted in pressure changes, phase boundary shifts and resorption, we see no reason to invoke processes such as magma mixing or assimilation. The various lithologies of Zagami might represent a good example of fractional crystallization in a closed system.

While it would be ideal to conduct experiments using the 'correct' bulk composition, that composition remains largely unconstrained, since the proportions of the various lithologies observed in the Zagami main mass is almost certainly not representative of the entire magma unit. Perhaps the best method for constraining the original melt composition is through studies of trapped melt inclusions, as was done for nakhlites by [22,23].

4. Dynamic crystallization experiments

We conducted nine dynamic crystallization experiments at different peak temperatures (1230º, 1240º, 1250ºC) and cooling rates (0.5º, 2º, 5º and 10ºC/h) to evaluate the importance of nuclei density and cooling rate on the crystallization of Zagami. While cooling rate has been the primary focus of the debate about the history of Zagami [6,7,12], nuclei density

is equally important in determining the final texture of basaltic rocks [15]. Cooling rates of 0.5–10ºC/h are representative of the range of cooling rates previously suggested (0.02–20ºC/h [6,7,12]). Simulation of slower cooling rates would have required unreasonably long experimental run times (e.g. 6 months). Nuclei densities are more difficult to constrain. We chose peak temperatures of 1250–1230ºC to produce small numbers of nuclei. Equilibrium experiments at these temperatures suggest nuclei abundances from ~1 wt.% (1250ºC) to ~3 wt.% (1230ºC). In experiments cooled from 1230º and 1240ºC, two charges were run simultaneously in the furnace. In many cases, differences were observed between the two charges, mostly in the degree of crystallization of the mesostasis. These differences likely reflect random nucleation events. In these cases, we selected the charge with the more crystallized mesostasis.

Brief descriptions of the experimental charges are given in Table 5 and photos of the charges are given in Fig. 2. Also shown in Fig. 2 is a transmitted light photomicrograph of Zagami to the same scale. Readers are referred [1,6,7,10,12] for a complete description of the textural, mineralogical and chemical features of the Zagami meteorite. One goal of this work is to determine the cooling rate and nuclei density at which Zagami might have formed. We have applied three criteria to determine the best match. These are (1) the overall texture of the charge, including grain sizes and shapes, (2) the morphology of the individual grains (skeletal vs. euhedral) and (3) the mineralogy of the mafic silicates (the presence of augite and pigeonite). Several trends are apparent in Table 5 and Fig. 2 and worthy of discussion. Experiments with abundant nuclei do not produce Zagami-like textures. Cooling at both 10º and 2ºC/h from 1230ºC, at which there would have been ~3% nuclei, produces numerous, small, semi-equant grains. Indeed, there is little textural difference between the two experiments, suggesting that nuclei density is the dominant control on texture at even moderate nuclei densities. Likewise, rapid cooling (10ºC/h) does not produce Zagami-like textures. Cooling at 10ºC/h from 1240ºC produces very skeletal grains with hollow cores, while cooling from 1250ºC produces a few, very skeletal orthopyroxenes in a fine, radiating textured charge. Choosing between the remaining charges is somewhat more difficult. Those cooled from 1240ºC tend to produce semi-equant grains and lack the elongate grains typical of shergottites. The experiment cooled from 1240ºC at 2ºC/h crystallized completely, with a mesostasis of major augite and plagioclase and minor whitlockite, Fe,Ti-oxides, SiO_2 and a myrmekitic SiO_2-Fe,Ti-oxide intergrowth. While this phase assemblage closely matches that seen in natural Zagami, texturally the rock is much more similar to Nakhla. Experiments cooled from 1250ºC tend to produce grains which become increasingly more euhedral with slower cooling rates and, thus, provide a better match with Zagami. We believe that the best match in our experimental set is provided by the charge cooled from 1250ºC at 0.5ºC/h. In this charge, the phenocryst phases are augite and pigeonite with semi-equant to elongate subhedral to euhedral forms. Both the grain sizes and shapes are similar to those in Zagami (Fig. 2). The matrix is largely glassy, but this reflects the difficulty of low-temperature experimental nucleation of phases and is not significant in determining the best match. It appears that Zagami likely formed from a melt with relatively low nuclei density at a slow cooling rate (<1ºC/h).

While our criteria for selecting a match between the experiments and Zagami were largely mineralogical and textural, it is important that we consider the chemical compositions of the pyroxene grains. We have examined zoning profiles in pyroxenes in the charge cooled from 1250ºC at 0.5ºC/h (exp. 038) (Figs. 3 and 4). Fig. 3 illustrates an augite grain from this experiment. This grain has core compositions of $Fs_{18–20}Wo_{28–30}$ and rim compositions up to $Fs_{33}Wo_{37}$. This experimental augite has compositions which are similar to augites in Zagami, which have core compositions of $Fs_{20}Wo_{34}$ and rim compositions of $Fs_{35}Wo_{33}$. In detail, there are important differences between this augite grain and augite in Zagami. In the center of the experimental grain, we observe a row of melt inclusions and a dramatic spike in the FeO concentration (an enrichment of ~4 wt.% FeO at ~300 μm). A smaller compositional spike (~3 wt.%) is observed closer to the edge of the grain (at ~500 μm). The FeO enrichment and row of magmatic inclusions strongly suggest a soda-straw growth mechanism, in which a hollow tube grows both inwards and outwards, trapping melt which

Table 5
Descriptions of dynamic crystallization experiments

Peak temp. (ºC)	Cooling rate			
	10ºC/h	5ºC/h	2ºC/h	0.5ºC/h
1250	**040** Large (up to 3 mm) skeletal to barred orthopyroxenes at bottom of charge. Remainder consists of very-fine dendrites of 2–10 μm wide skeletal augite and Fe,Ti-oxides set in glass.	**042** Pyroxenes are subhedral to anhedral and range from small (~100 μm) semi-equant grains to laths up to 2 mm in length. The pyroxenes are complex intergrowths of augite to subcalcic augite. Minor gravitational settling is observed. A single olivine grain was also found. The groundmass is completely glassy and lacks any crystals of Fe,Ti-oxides or augite.	**034** Pyroxenes range from euhedral grains of a few hundred microns to slightly skeletal laths up to 3 mm in length. Grains are complex augite–pigeonite intergrowths. Groundmass is completely glassy and lacks any crystals of Fe,Ti-oxides or augite.	**038** Pyroxenes range from euhedral grains of a few hundred microns to slightly skeletal laths up to 3.5 mm in length. Gravitational settling of pyroxenes is apparent. Grains are complex augite–pigeonite intergrowths. Groundmass is largely glass with abundant 10–100 μm subhedral to skeletal Fe,Ti-oxides.
1240	**062B** Pyroxenes range from small (0.2 mm), subhedral, semi-equant grains to large (1.5 mm) laths. Pyroxenes are complex intergrowths of augite and pigeonite; often pigeonite grains with hollow cores infilled by augite. No obvious gradation in size. Glassy groundmass with skeletal 10–50 μm augites and Fe,Ti oxides.		**052F** Pyroxenes range from small (0.1 mm), subhedral, semi-equant grains to large (1 mm) elongate grains. Pyroxenes are complex intergrowths of augite and pigeonite; occasional pigeonite grains with hollow cores infilled by augite. No obvious gradation in size. Crystalline radiating groundmass of major augite and acicular plagioclase and minor whitlockite, Fe,Ti-oxides, SiO_2 and a myrmekitic SiO_2-Fe,Ti-oxide intergrowth.	**068B** Highly graded with pyroxenes ranging from small (50 μm), subhedral to anhedral, semi-equant grains to large (1 mm) semi-equant to elongate grains. Pyroxenes are complex intergrowths of augite and pigeonite; pigeonite grains infilled by augite. Groundmass is almost completely glassy with rare ~5 μm subhedral Fe,Ti-oxides.
1230	**046B** Semi-equant, subhedral to anhedral pyroxenes grading from ~50 μm at bottom to ~500 μm at top of charge with most grains ~100 μm. Pyroxenes are complex intergrowths of augite and pigeonite. Groundmass is largely glass with 10–20 μm Fe,Ti-oxides and augite laths.		**048A** Semi-equant, subhedral to anhedral pyroxenes grading from ~50 μm at bottom to ~500 μm at top of charge with most grains ~100 μm. Pyroxenes are complex intergrowths of augite and pigeonite. Slightly more crystallized than exp. 046B. Groundmass is largely glass with 10–50 μm Fe,Ti-oxides and rare augite laths.	

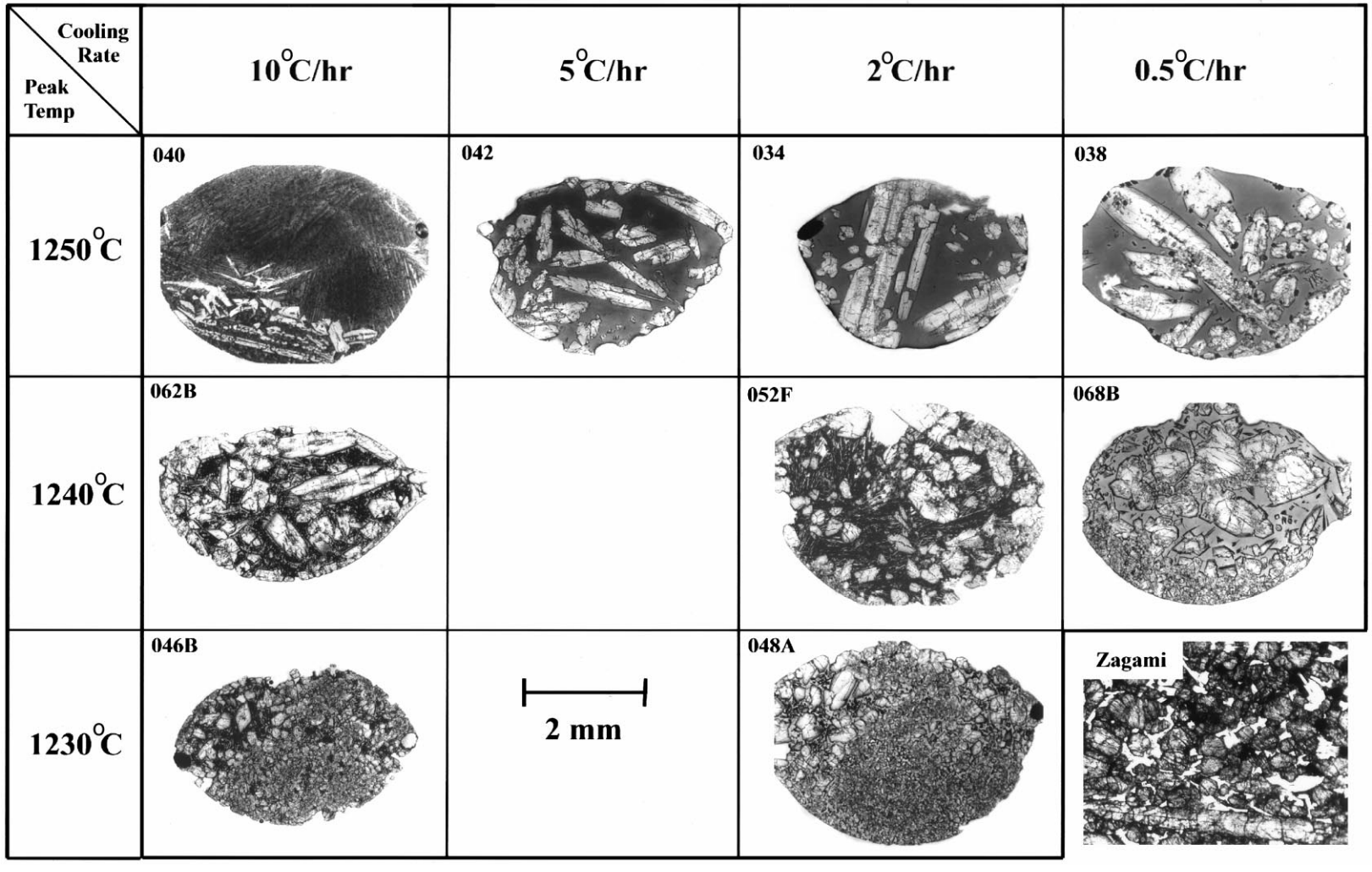

Fig. 2. Experimental charges produced at a range of cooling rates (0.5–10ºC/h) and peak temperatures (1250–1230ºC), which serve to change the nuclei density from ~1 to 3 vol.%. Zagami is shown at the same scale. The overall texture, grain sizes and shapes and mineralogy is best replicated during cooling from 1250ºC at 0.5ºC/h, consistent with the suggestions of [7,12] that Zagami cooled at >1ºC/h.

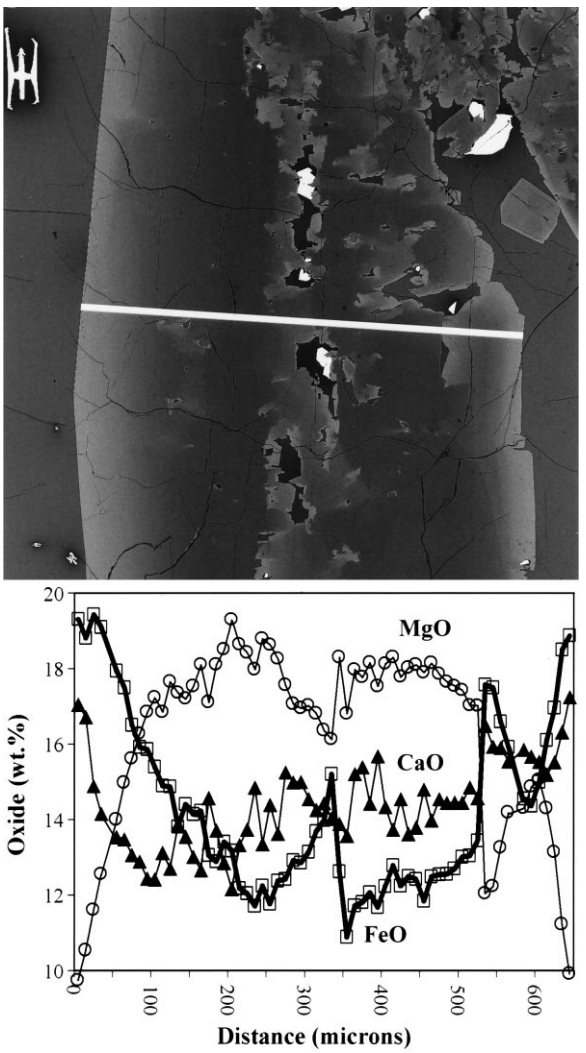

Fig. 3. Back-scattered electron image of an augite crystal from the experiment cooled from 1250ºC at 0.5ºC/h. White line is the trace of the zoning profile shown below. The grain ranges from $Fs_{\sim 20}$ at the core to $Fs_{\sim 33}$ at the rim, similar to those in Zagami. However, the center of the grain is FeO-enriched and contains numerous melt inclusions, indicative of soda-straw growth. FeO-enrichments of this magnitude and the abundant melt inclusions observed in the experiment are not seen in Zagami.

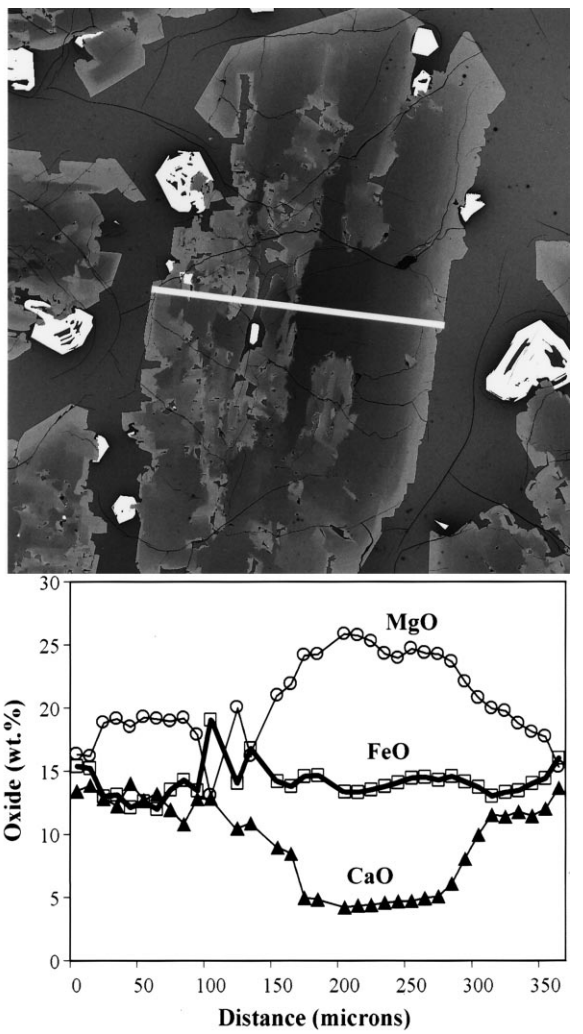

Fig. 4. Back-scattered electron image of a compound pigeonite–augite crystal from the experiment cooled from 1250ºC at 0.5ºC/h. White line is the trace of the zoning profile shown below. The pigeonite is FeO-poor ($Fs_{\sim 20}$) compared to the magnesian cores of pigeonite in Zagami ($Fs_{\sim 30}$). Both the zoning and nature of the intergrowths is much more ragged in this grain than has been observed in Zagami.

fractionally crystallizes FeO-rich pyroxene. Alternatively, the irregular intergrowths might result from resorption of early-formed magnesian pyroxene and subsequent crystallization of iron-enriched pyroxene. While skeletal growth might explain entrapment of melt inclusions in Zagami [6], the abundance of melt inclusions and iron enrichment in the center of this experimental grain have not been observed in natural Zagami [6,7], suggesting that Zagami crystallized even slower than this experiment (<0.5ºC/h).

A more dramatic mismatch is observed in the pyroxenes which contain both augite and pigeonite (Fig. 4). These pyroxenes tend to be extremely complex intergrowths of the two phases. The core

of this grain is pigeonite with a composition of $Fs_{20–22}Wo_{8–10}$. This is significantly more FeO-poor than observed in Zagami, where magnesian pigeonite cores have compositions around $Fs_{30}Wo_{13}$. The rims of this grain are augite with complex, ragged zoning profiles. Again, this is unlike that observed in Zagami [6,7]. Fe zoning across a grain which contained both augite and pigeonite had ∪-shaped zoning profiles in both portions of the grain [6]. In contrast, the experimental augite–pigeonite grain has nearly flat FeO zoning, with the exception of FeO spikes at the augite–pigeonite boundary.

While slow cooling with relatively few nuclei produces textures and mineralogies comparable to Zagami, it is clear that important differences remain in the detailed chemical compositions and zoning of these grains. What is the source of these differences? The most obvious explanation is that Zagami crystallized from a magma of different composition than used in these experiments. This is the preferred explanation for differences between core abundances in our equilibrium experiments and Zagami. The major difference postulated between the composition we used and the one from which Zagami likely crystallized is that the latter had a higher Fe/Mg ratio. Would this affect the crystallization behavior of the experiments? Certainly a melt with a higher Fe/Mg ratio would initially crystallize more FeO-rich pyroxene, perhaps reducing the discrepancy between the most magnesian pigeonite in the dynamic crystallization experiments ($Fs_{20–22}Wo_{8–10}$) and the most magnesian pigeonite composition in Zagami ($Fs_{30}Wo_{13}$). It is less clear whether a change in the Fe/Mg ratio would produce a significant change in the morphology of the grains. In particular, the experimental grains remain extremely ragged with numerous melt inclusions relative to those in Zagami. It is difficult to predict how a change in composition would affect the texture of the crystallizing melt. Factors such as network former/modifier ratio, diffusion rates in the silicate melt, susceptibility to undercooling and phase relationships are all linked directly or indirectly to composition and all affect texture. It seems unlikely that Fe/Mg ratio would change the network former/modifier ratio, as Fe and Mg have comparable behaviors in forming and modifying networks [24]. The Fe/Mg ratio could certainly affect the phase relations. For example, reducing the temperature interval between crystallization of pigeonite and augite would likely increase the number of nuclei in the melt and decrease the average grain size (e.g. [15]). Although experiments with a different Fe/Mg ratio would be interesting, the exact composition from which Zagami crystallized remains largely unconstrained, as discussed above.

An equally likely explanation is that we have not adequately duplicated the thermal history experienced by Zagami. Three possibilities for the cooling history include: (a) Zagami cooled at a constant rate (e.g. 0.01ºC/h from the liquidus to the solidus); (b) the cooling rate decreased with time (e.g. 0.1ºC/h above the solidus to 0.01ºC/h subsolidus); or (c) a two-stage cooling history is required (e.g. nearly isothermal crystallization near the liquidus followed by moderate cooling (0.1ºC/h). A slower cooling rate (case a) is consistent with the suggestions of [7,12] that Zagami cooled at rates of a tenth to a hundredth of a degree per hour. In our constant cooling rate experiments, we observed increasingly subhedral to euhedral grains with fewer melt inclusions as the cooling rate decreased from 10º to 0.5ºC/h. Slower cooling rates, perhaps with undercooling, are likely to produce more equant crystals by infilling of originally skeletal crystals [15] and the zoning profiles are likely to become more ∪-shaped with slower cooling. The exact interplay between cooling rate and undercooling might produce originally skeletal crystals. The case of a decreasing cooling rate with time (case b) is more likely if extrapolated to subsolidus temperatures. In this case, solid state diffusion might smooth zoning profiles, producing some of the chemical zoning features observed in Zagami. A two-stage cooling history (case c) might be able to better duplicate the zoning patterns if homogeneous magnesian pyroxenes of sufficient size can be grown under essentially isothermal conditions. Thus, the question of a one-stage vs. two-stage crystallization history must await experiments at slower cooling rates and determination of the melt composition from which Zagami crystallized. Slower cooling rates could not be experimentally reproduced because of the substantial times needed (5 months for cooling rates of 0.1ºC/h to 4 years for a cooling rate of 0.01ºC/h).

5. Conclusions

(1) Our equilibrium experiments yield results similar to those of [1] and the difference between experimental studies, which produce ~40 wt.% magnesian pyroxene, and petrologic studies, which observe 10–20 wt.%, remains.

(2) Crystallization of Zagami under slightly more reducing conditions than QFM is unable to explain this discrepancy.

(3) This and previous studies [6,7,10,12] suggest that Zagami crystallized from a melt enriched in Fe/Mg relative to our starting composition and that resorption of pyroxenes played an important role in the formation of Zagami.

(4) Zagami formed from a melt with a low nuclei density ($\leq$1 vol.%) at a relatively slow cooling rate ($<$0.1°C/h). This favors either thick lava flows or a subsurface origin and suggests that rocks like Zagami are not likely to sample the outer portions of lava flows accessible in situ by Mars missions, although they may be sampled as impact ejecta.

(5) The bulk composition from which Zagami crystallized and the exact combination of cooling rate and nuclei density from which it forms remain unknown.

Acknowledgements

We gratefully recognize the assistance of L. Le, A. Jurewicz, V. Lauer, J. Wagstaff, C. Schwandt, V. Yang, P. Bernhard, E. Jarosewich, A. Logan and Y. Guan in conducting the experiments, preparing polished thin sections and performing microprobe analyses. Enlightening discussions with V.P.S. Hale are appreciated. Thoughtful reviews by R. Harvey, H. McSween Jr., and A. Treiman significantly improved the manuscript. This work was supported by a National Research Council Postdoctoral Fellowship to TJM and NASA grants NAG 5-4490 (TJM) and RTOP 344-31-20-20 (GEL). ***[AH]***

References

[1] E.M. Stolper, H.Y. McSween Jr., Petrology and origin of the shergottite meteorites, Geochim. Cosmochim. Acta 43 (1979) 1475–1498.

[2] M.B. Duke, The Shergotty meteorite: magmatic and shock metamorphic features, in: B.M. French, N.M. Short (Eds.), Shock Metamorphism of Natural Materials, Mono Book Corp., Baltimore, MD, 1968, pp. 613–621.

[3] J.V. Smith, R.L. Hervig, Shergotty meteorite: mineralogy, petrology, and minor elements, Meteoritics 14 (1979) 121–142.

[4] H.Y. McSween Jr., E. Jarosewich, Petrogenesis of the Elephant Moraine A79001 meteorite: multiple magma pulses on the shergottite parent body, Geochim. Cosmochim. Acta 47 (1983) 1501–1513.

[5] A.H. Treiman, Amphibole and hercynite spinel in Shergotty and Zagami: magmatic water, depth of crystallization, and metasomatism, Meteoritics 20 (1985) 229–243.

[6] A.H. Treiman, S.R. Sutton, Petrogenesis of the Zagami meteorite: inferences from synchrotron X-ray (SXRF) microprobe and electron microprobe analyses of pyroxene, Geochim. Cosmochim. Acta 56 (1992) 4059–4074.

[7] T.J. McCoy, G.J. Taylor, K. Keil, Zagami: product of a two-stage magmatic history, Geochim. Cosmochim. Acta 56 (1992) 3571–3582.

[8] M. Wadhwa, H.Y. McSween Jr., G. Crozaz, Petrogenesis of shergottite meteorites inferred from minor and trace element microdistributions, Geochim. Cosmochim. Acta 58 (1994) 4213–4229.

[9] V.P.S. Hale, H.Y. McSween Jr., G.A. McKay, Re-evaluation of intercumulus liquid composition and oxidation state for the Shergotty meteorite, Geochim. Cosmochim. Acta 63 (1999) 1459–1470.

[10] T.J. McCoy, M. Wadhwa, K. Keil, New lithologies in the Zagami meteorite: evidence for fractional crystallization of a single magma unit on Mars, Geochim. Cosmochim. Acta 63 (1999) 1249–1262.

[11] G. McKay, J. Wagstaff, S.-R. Yang, Clinopyroxene REE distribution coefficients for shergottites: the REE content of the Shergotty melt, Geochim. Cosmochim. Acta 50 (1986) 927–937.

[12] A.J. Brearley, Subsolidus microstructures and cooling history of pyroxenes in the Zagami shergottite (abstr.), Lunar Planet. Sci. 22 (1991) 135–136.

[13] G.E. Lofgren, C.H. Donaldson, T.M. Usselman, Geology, petrology, and crystallization of Apollo 15 quartz-normative basalts, Proc. Lunar Planet. Sci. Conf. 6 (1975) 79–99.

[14] F.G.F. Gibb, Supercooling and the crystallization of plagioclase from a basaltic magma, Min. Mag. 39 (1974) 641–653.

[15] G.E. Lofgren, Effect of heterogeneous nucleation on basaltic textures: a dynamic crystallization study, J. Petrol. 24 (1983) 229–255.

[16] A. Kouchi, A. Tsuchiyama, I. Sunagawa, Effect of stirring on crystallization kinetics of basalt: texture and element partitioning, Contrib. Mineral. Petrol. 93 (1986) 429–438.

[17] S. Ghosal, R. Sack, M.S. Ghiorso, M.E. Lipschutz, Evidence for a reduced, Fe-depleted Martian mantle source region of shergottites, Contrib. Mineral. Petrol. 130 (1998) 346–357.

[18] M. Hashimoto, G. McKay, L. Le, C. Schwandt, T. Mikouchi, Experimental crystallization of a revised Shergotty bulk composition (abstr.), Meteoritics Planet. Sci. 34 (1999) A51–A52.

[19] R.K. Popp, D. Virgo, H.S. Yoder Jr., T.C. Heoring, M.W. Phillips, An experimental study of phase equilibria and Fe oxy-component in kaersutitic amphibole: implications for the f_{H2} and a_{H2O} in the upper mantle, Am. Mineral. 80 (1995) 534–548.

[20] R.K. Popp, D. Virgo, M.W. Phillips, H deficiency in kaersutitic amphiboles: experimental verification, Am. Mineral. 80 (1995) 1347–1350.

[21] R.A. Robie, B.S. Hemingway, J.R. Fisher, Thermodynamic Properties of Minerals and Related Substances at 298.15 K and 1 Bar (10^5 Pascals) Pressure and at Higher Temperatures, U.S. Geol. Surv. Bull. 1452 (1978) 456 pp.

[22] R.P. Harvey, H.Y. McSween Jr., The parent magma of the nakhlite meteorites: clues from melt inclusions, Earth Planet. Sci. Lett. 111 (1992) 467–482.

[23] A.H. Treiman, The parent magma of the Nakhla (SNC) meteorite, inferred from magmatic inclusions, Geochim. Cosmochim. Acta 57 (1993) 4753–4767.

[24] P.C. Hess, Polymerization model for silicate melts, in: R.B. Hargraves (Ed.), Physics of Magmatic Processes, Princeton Univ. Press, Princeton, NJ, 1980, pp. 3–48.